ADVANCED MATERIALS INTERFACES
Open Access
www.advmatinterfaces.de

Impact of Twin's Landscape on the Magnetic Damping of $La_{2/3}Sr_{1/3}MnO_3$ Thin Films

*Shoulong Chen, Alberto Pomar, Lluis Balcells, Carlos Frontera, Narcís Mestres, and Benjamín Martínez**

Understanding the origin and mechanisms of magnetic damping in complex oxide materials is crucial for optimizing spin dynamics and tailoring their properties for specific spintronic applications. Ferromagnetic resonance spectroscopy (FMR) technique has been used to investigate the magnetic damping of multiple $La_{2/3}Sr_{1/3}MnO_3$ (LSMO) epitaxial thin films with similar thickness and identical DC magnetic properties. However, the dynamic magnetic properties exhibit noticeable variations among samples. Microstructural analyses using X-ray diffraction (XRD) and atomic force microscopy (AFM), confirm that the samples are structurally identical, except for minute differences in the miscut angles of the substrates. Nevertheless, when examining the samples using backscattered electron (BSE) images in scanning electron microscopy (SEM), significant disparities in the twin distribution are observed. These variations in the twin distribution directly correlate with the observed differences in the damping values. A careful image analysis of BSE images allows to demonstrate that the increase of damping is due to the pinning of the magnetization in the twin boundaries.

1. Introduction

Spintronics is a rapidly growing field of research that involves the generation, manipulation, and control of the spin of electrons in materials. These have the potential to revolutionize information technology by providing faster, more efficient, and more versatile ways of processing and storing information.[1,2] To reach these objectives materials used in spintronics must possess specific characteristics to enable efficient manipulation and control of electron spins. Materials with long spin diffusion lengths are desirable as they facilitate efficient spin transport over larger distances. In addition, low magnetic damping coefficients are also crucial for attaining efficient spin transfer, preserving spin coherence, and lowering energy dissipation.[3,4,5] Thus, controlling and minimizing magnetic damping is essential for achieving efficient spin dynamics and transport in spintronic devices.[2,4] However, low-damping materials are scarce; ferrimagnetic insulators, such as Yttrium-iron-garnet (YIG), use to exhibit very low damping due to the absence of conduction electrons, which suppress the magnon-electron scattering but, their applications are limited by their insulating nature.[6,7] Finding ferromagnetic metallic materials with low damping is a complex task because of the scattering of magnons by the conduction electrons. Heusler alloys are an example of this kind of materials with damping values typically in the range 1×10^{-3} to 4×10^{-3} however, their special preparation requirements limit their possible applications.[8,9] In this context, complex oxides have gained significant attention in recent years since they can combine a relatively low damping with a wide range of magnetic and electronic properties that can be tuned by controlling the crystal structure or composition of the material.[10,11] In particular, $La_{2/3}Sr_{1/3}MnO_3$ (LSMO) compound has been the subject of intense research due to its half-metallic ferromagnetic character and predicted related low damping.[12,13] Nevertheless, its magnetic dynamic properties are still to be well established. Previous reports gave values of damping of LSMO films that are clearly larger than 1×10^{-3},[14,15,16] and only go down to 10^{-4} range for sample thickness of ≈40–50 nm and above.[17,18]

Magnetization dynamics is usually described by the Landau–Lifshitz–Gilbert (LLG) equation that takes magnetic damping into account in a phenomenological manner.[19] In the attempt to unveil the physical origin of the damping, models, such as Kambersky's breathing Fermi surface (BFS) and torque-correlation models (TCM),[20,21] have been introduced. These models explicitly incorporate spin-orbit coupling, a crucial factor in the energy transfer between magnetization and electronic degrees of freedom, and have shown to be effective in capturing the important physical effects involved in precession damping. However, they fail to establish a clear relationship with the physical properties of the material and how to influence damping through its modification.[3,22] Further developments based on these two models (BFS and TCM) have revealed a close

S. Chen, A. Pomar, L. Balcells, C. Frontera, N. Mestres, B. Martínez
Instituto de Ciencia de Materiales de Barcelona
ICMAB-CSIC
Campus Universitario UAB, Bellaterra 08193, Spain
E-mail: ben.martinez@icmab.es

The ORCID identification number(s) for the author(s) of this article can be found under https://doi.org/10.1002/admi.202300882

DOI: 10.1002/admi.202300882

correlation between damping and density of states and spin-orbit coupling strengths.[22] In complex oxides, such as LSMO, several factors can affect the magnetic damping. These factors encompass the lattice structure, defects, interfaces, and electron-electron interactions. They have the potential to enhance the scattering rate between electrons and the lattice, introduce local scattering centers in the form of magnetic inhomogeneities, modify the density of states, and alter the effective spin-orbit parameter thus, affecting the magnetic damping. In particular, in epitaxial LSMO thin films misfit strain affects the deformation of perovskite-type ABO_3 octahedral frameworks therefore, modifying the delicate balance between lattice, spin, charge, and orbital degrees of freedom.[23] Epitaxial LSMO films grown onto (001) oriented $SrTiO_3$ (STO) substrates are under biaxial tensile stress imposed by the accommodation of the incommensurate rhombohedral lattice of bulk LSMO to the STO cubic substrate. This process implies an intricate relaxation pattern that involves a complex rotation and deformation of corner-sharing BO_6 octahedra that changes as a function of the film thickness affecting the magnetic anisotropy,[23,24] and therefore the magnetic damping. A typical mechanism for misfit strain relaxation in LSMO thin films of about 10 nm thick and above is twinning.[25] This relaxation mechanism gives place to the formation of a twin domain pattern and the appearance of twin boundaries, i.e., interfaces separating regions of the LSMO film with different crystallographic orientations. These twin boundaries can have a significant impact on the film's electronic and magnetic properties and its abundance and distribution may be modified by subtle changes during the postgrowth annealing processes.

In this study, we investigate the magnetic damping of multiple LSMO samples with similar thickness and DC magnetic properties. However, despite having identical DC magnetic properties, the dynamic magnetic properties exhibit noticeable variations among the samples. We conduct microstructural analyses using X-ray diffraction (XRD) and atomic force microscopy (AFM), confirming that the samples are structurally identical, except for minute differences in the miscut angles of the substrates.

Nevertheless, when examining the samples through backscattered electron (BSE) images in scanning electron microscopy (SEM) , we observe significant disparities in the twins' distribution. These variations in the distribution of twins directly correlate with the observed differences in the damping values. Samples that possess only one family of twins display a narrow ferromagnetic resonance (FMR) linewidth and a uniaxial anisotropy term superimposed to the usual in-plane fourfold anisotropy found in LSMO thin films under tensile strain. In contrast, in the samples containing two families of twins, the uniaxial anisotropy term is absent exhibiting only the usual in-plane fourfold anisotropy, where the hard magnetization axis aligns along the [100] and [010] directions. In addition, these samples show a broader FMR linewidth and therefore, higher magnetic damping. A careful image analysis of BSE images allows to demonstrate that the increase of damping is due to the pinning of the magnetization in the twin boundaries.

2. Experimental

A set of LSMO samples with a thickness of 11–15 nm have been prepared by RF sputtering on top of (001)-oriented $SrTiO_3$ (STO) single-crystal substrates. LSMO films were deposited at 850 °C and 140 mTorr of pressure in an Ar-O_2 atmosphere. Then, the films were annealed at 850 °C in high-pressure oxygen atmosphere (380 Torr). Structural features of the samples were studied by XRD, X-ray reflectometry (XRR) and AFM measurements. The static magnetic properties of the LSMO films were studied using a SQUID magnetometer by Quantum Design. The diamagnetic signal of the substrate and other instrumental contributions for DC magnetization measurement were properly corrected.[26] The dynamic magnetic properties of the LSMO thin films were studied by means of FMR using a commercial broadband coplanar waveguide (CPW) (by NanOsc) inserted into a physical properties measurement system (PPMS by Quantum Design).

X-ray microstructural characterization reveals that the samples are epitaxial and growing on a cube-on-cube orientation relationship onto the STO substrate, [100]LSMO//[100]STO (pseudocubic indexation is used throughout for simplicity) (see Supporting Information). AFM measurements show that the surfaces of the different samples are very similar with surface roughness of about 0.2 nm. All these studies indicate that samples are structurally identical, except for minute differences in the miscut angles of the substrates, that has no measurable influence on the magnetic properties of the samples. X-ray reciprocal space maps (RSM) around the (1 0 3) reflection of the STO substrate show that films grow with in-plane lattice parameters well matched to the STO substrate, and without evidence of lattice relaxation (see Supporting Information).

However, BSE images of the surface of the different samples exhibit significant disparities in the twin distribution, as shown in **Figure 1**. It can be clearly appreciated that the distribution of twin domains is substantially different from one sample to another.

On the other hand, the temperature dependence of magnetization, normalized to the value at T = 10 K (all the samples exhibit saturation magnetization (M_S) values close to that corresponding to the theoretical value ($M_S \approx 580$ emu cm^{-3})), corresponding to the same set of samples is shown in **Figure 2a**. The figure demonstrates that, concerning DC magnetic properties, all the samples exhibit a very similar behaviour, i.e., similar T_C and M_S.

However, a detail of the hysteresis loops in the low field regime (see Figure 2b) make evident that in the case of sample A, both the hysteresis cycle and the approach to saturation process differ from the others, suggesting a subtle variance in the magnetic anisotropy. Hence, considering the DC magnetic properties, it can be inferred that all the samples share a similar behavior. Next, we proceed with the study of the dynamic magnetic properties by using the FMR technique. FMR measurements were performed by sweeping the externally applied magnetic field, H, in the microwave range from 2 to 16 GHz. The external static magnetic field was applied in-plane. In **Figure 3** the field derivatives of the FMR absorption lines, at room temperature, corresponding to some of the samples in Figure 1 are depicted. The figure makes evident a clear broadening of the resonance linewidth, ΔH, closely related to the magnetic damping of the system, that correlates with the abundance of twin boundaries in each sample according to the results shown in Figure 1.

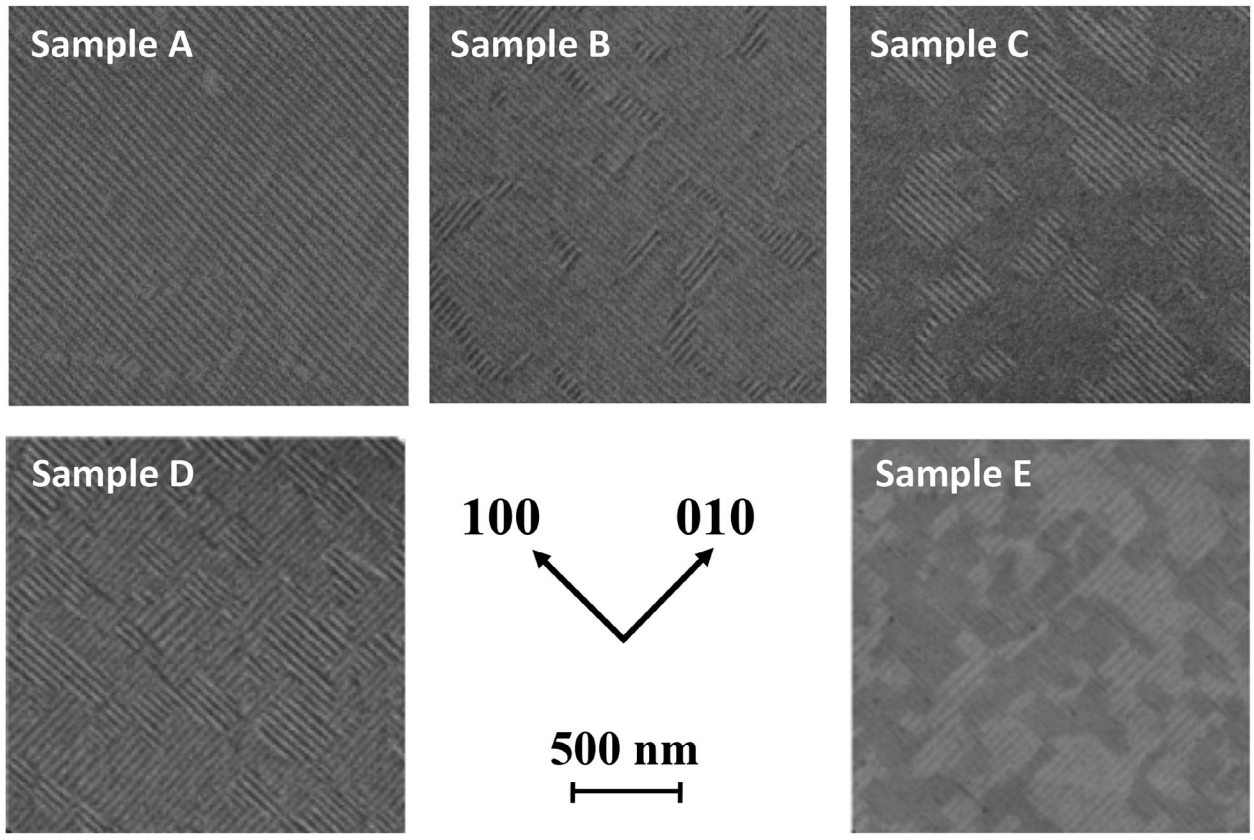

Figure 1. BSE images of several LSMO thin films displaying diverse distributions of twin domains. The twin formations manifest as parallel stripes exhibiting alternating dark or bright contrasts, aligning with the [100] and [010] film directions.

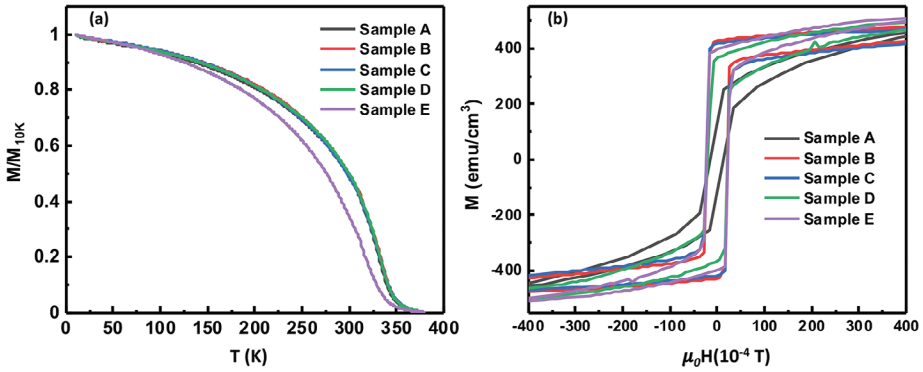

Figure 2. a) Temperature dependence of the magnetization for LSMO thin films. For comparison, values have been normalized by the corresponding magnetization at 10 K. b) Hysteresis loops at T = 10 K.

3. Results and Discussion

FMR curves at different frequencies were fitted according to the expression:

$$\frac{dS}{dH} = \frac{d}{dH}\left[\frac{k_s \Delta H^2}{\Delta H^2 + 4\left(H - H_{\text{res}}\right)^2} + \frac{k_{as}\Delta H\left(H - H_{\text{res}}\right)}{\Delta H^2 + 4\left(H - H_{\text{res}}\right)^2}\right] \quad (1)$$

where dS/dH is the field-derivative of the absorption peak, k_s and k_{as} are the (dimensionless) symmetric and antisymmetric amplitudes, respectively, and H_{res} is the resonance field. From the frequency dependence of ΔH and H_{res} dynamic and static magnetic parameters of the LSMO film, such as the gyromagnetic ratio γ, the effective magnetization M_{eff} and the Gilbert damping parameter, α, can be determined. When magnetic field is applied in-plane parallel to an easy axis direction, the resonance frequency, f_{res}, and H_{res} are related through the in-plane Kittel equation:[27]

$$f_{res} = \frac{\gamma}{2\pi}\left(H_{res} + \frac{2K_4}{M_S}\right)^{1/2} \cdot \left(H_{res} + 4\pi M_{eff} + \frac{2K_4}{M_S}\right)^{1/2} \quad (2)$$

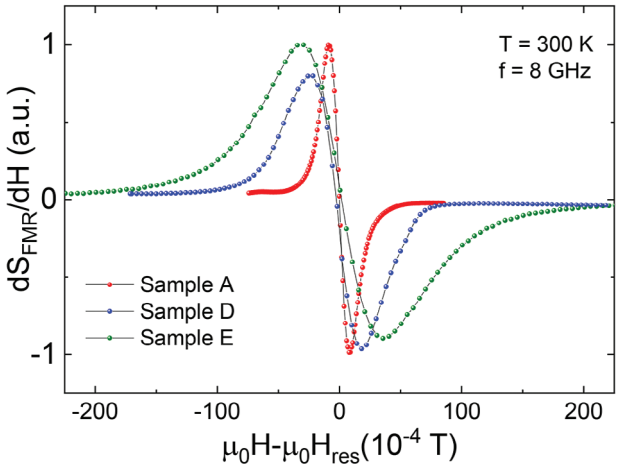

Figure 3. Field derivatives of the FMR absorption peaks corresponding to some of the samples exhibiting distinct twin structures (see Figure 1) taken at 300 K and 8 GHz.

where K_4 is the fourth-order term of the magnetic anisotropy that, as mentioned above, is typically present in LSMO thin films, and M_{eff} is the effective magnetization. This effective magnetization can be expressed as $4\pi M_{\text{eff}} = 4\pi M_S - 2K_2/M_S$, being K_2 the second-order or surface/interface anisotropy constant and M_S the saturation magnetization of the LSMO film, which opposes the demagnetizing field. The linewidth of the FMR spectra is described by a linear dependence on the resonance frequency:

$$\Delta H = \Delta H(0) + \frac{2\pi}{\gamma}\alpha f_{res} \tag{3}$$

Being $\Delta H(0)$ the so-called inhomogeneous line broadening or damping, which is nearly zero for magnetically and structurally homogeneous systems, and α the Gilbert damping parameter. To further investigate the effect of the twins on the dynamic response, FMR measurements were carried out with the magnetic field applied parallel to the main crystallographic directions of the substrate. Characteristic FMR spectra recorded at 8 GHz while applying the magnetic field parallel to the substrate edges ([100] and [010] directions) at room temperature are shown in **Figure 4**. The spectra pertain to two distinct samples: one containing a single family of twins (Sample A in Figure 1), and the other encompassing both twin families, thus exhibiting different twin domains (Sample D in Figure 1).

Figure 4 provides clear evidence that sample A, which comprises only one family of twins, i.e., without twins' boundaries, exhibits distinct anisotropic behavior, as already intuited from the slightly distinct hysteresis loop. In contrast, samples containing both families of twins, i.e., containing a distribution of twin' boundaries, display primarily isotropic characteristics. Interestingly, despite the anisotropic behavior observed in sample A, it's noteworthy that the value of α is the same regardless of the orientation of the magnetic field (see Figure 4b).

To clarify the impact of twins on the observed increase of α and the anisotropic dynamic magnetic behavior, FMR measurements with the DC magnetic field applied parallel to the main crystallographic directions of the substrate (see Figure 4) have been performed. In the case of sample A, which contains only one family of twins (see Figure 1), the FMR measurements yielded orientation-dependent resonant field values (see Figure 4a). These findings provide direct evidence of a dominant uniaxial anisotropy, H_u, with the hard magnetization axis aligned along [100], i.e., parallel to the twin' walls. On the other hand, FMR spectra corresponding to sample D, which possesses both families of twins (see Figure 1), did not show any significant orientation-dependent shift of the resonance fields (see Figure 4c). Thus, it can be inferred that, in this sample, H_u is negligible at room temperature. At this point it is convenient to recall what is known regarding magnetic anisotropy in the LSMO system. Previous research on LSMO single crystals has revealed the presence of a uniaxial in-plane magnetic anisotropy stemming from magnetocrystalline anisotropy.[28,29] However, in the case of LSMO thin films, epitaxial stress induced by the substrate can introduce an additional source of anisotropy, i.e., magnetoelastic anisotropy, alongside the crystalline anisotropy. Specifically, when LSMO epitaxial films are grown on (001) STO substrates, the tensile epitaxial stress exerted by the substrate results in a tetragonal symmetry,[30] which is compatible with the already reported fourfold in-plane magnetic anisotropy with the easy axis along ⟨110⟩.[24,31] Since LSMO films used in this study are in-plane fully strained, it is natural to assume that they also present fourfold in-plane magnetic anisotropy with hard axes along tetragonal ⟨100⟩, assumption that is compatible with the results shown in Figure 4c. In fact, the value of H_{res} along the [010] direction in sample A is similar to H_{res} values in sample D which suggests similar values of anisotropy. According to this, sample A would present and extra dominant uniaxial anisotropy term with the hard direction along the [100].

To take into account the effect of this additional anisotropy term Equation (2) has been conveniently modified to include an extra anisotropy field, H_u, term. The resulting expression, for in-plane measurements, may be written as:

$$f = \frac{\gamma}{2\pi}\mu_0\left[H_{res} + H_u\cos 2\emptyset_u + H_4\cos 4\emptyset_4\right]^{1/2}$$
$$\left[H_{res} + 4\pi M_{eff} + \frac{1}{2}H_u\left(1 + 2\cos 2\emptyset_u\right) + \frac{1}{4}H_4\left(3 + \cos 4\emptyset_4\right)\right]^{1/2} \tag{4}$$

where $\varnothing_u$ and $\varnothing_4$ are the angles between the applied magnetic field and the corresponding easy axis associated to H_u and H_4 anisotropy fields. According to this, the frequency dependence on the resonant field has been analyzed using Equation (4). Using the above expression, we have obtained that, for sample A, at room temperature, $H_u(=2K_u/M_s) \approx 37$ Oe which yields an anisotropy constant of $K_u = 5.4\times10^3$ erg cm^{-3}, while H_u is negligible for the rest of the samples. Furthermore, it is found that in all the samples H_4(300K) ($=2K_4/M_s$) is estimated to be below 7 Oe (i.e., $K_4<1\times10^3$ erg/cm^3 at room temperature). It's noteworthy to highlight that the in-plane fourfold anisotropy constant obtained from our measurements closely aligns with values documented in the literature for LSMO films of comparable thickness grown on (001)STO substrates.[24,31] In order to understand the origin of this uniaxial anisotropy term, it is convenient to review the structure of the twins in the LSMO. As shown in our previous work,[32,33] the twins have a precise structure in which the central

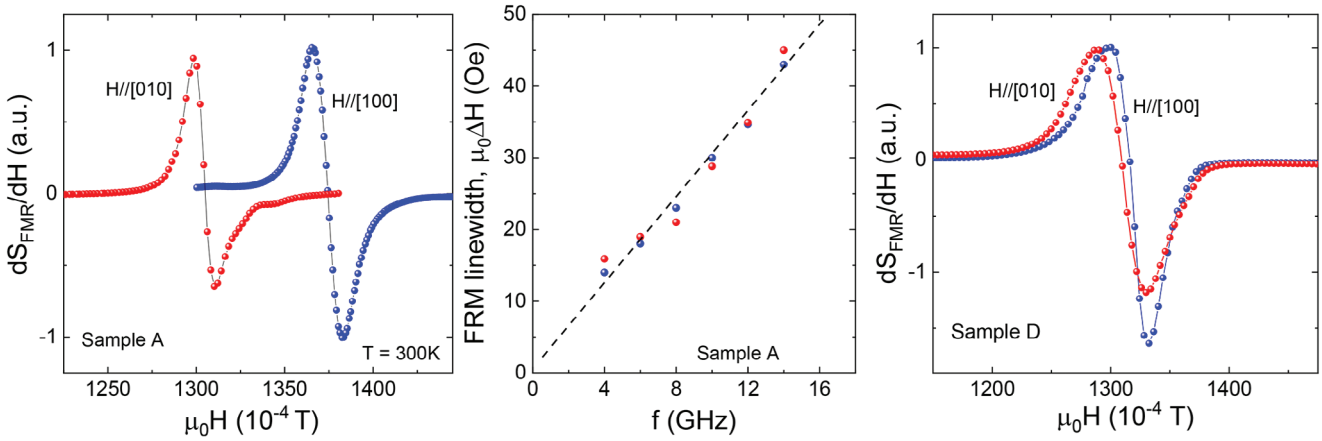

Figure 4. a) Field derivatives of the FMR absorption lines corresponding to sample A with the magnetic field applied parallel to the twins' walls ([100] direction) and perpendicular to them ([010] direction) taken at 300K and 8 GHz. b) Dependence of the FMR linewidth, ΔH, on the resonance frequency for sample A with the magnetic field applied along the [100] and [010] directions. c) Field derivatives of the FMR absorption lines corresponding to sample D with the magnetic field applied along the [100] and [010] directions

part (twin wall (TW)) is strongly distorted and has a cubic structure that relaxes progressively on both sides in the twin domain. Therefore, the twinned film can be viewed as a self-organized nanostructure consisting of ≈1 nm thick sheets of strongly compressed LSMO (the TW) embedded in an LSMO matrix subjected to tensile stress in the direction perpendicular to the TWs that go alongside the (100) or (010) directions.[32] Since in LSMO magnetostriction is positive,[34] the easy axis occurs when the magnetization is parallel to the stress axis, i.e., perpendicular to the TWs, as observed in sample A. In contrast, in the rest of the samples, since both twin families are present, this effect is washed out leaving the fourfold in-plane anisotropy term as the predominant effect.

4. Conclusions

Once the source of the uniaxial anisotropy observed in sample A has been established, our attention will shift toward examining the changes in damping. As illustrated in Figure 1, the emergence of the two distinct twin families inherently results in the appearance of boundaries between twinning domains. The biaxial tensile stress imposed by the STO cubic substrate generates an equal in-(out-) phase rotation of the MnO_6 octahedra along the *a*-(*b*) axis, without rotation along the *c*-axis. Given that the octahedra rotation directions within each twin family are opposite and that the physical properties of LSMO are strongly dependent on the MnO_6 octahedra arrangement, these twin boundaries will generate zones characterized by pronounced distortions in magnetic interactions. These distortion zones can serve as effective pinning centers for magnetization, consequently amplifying the damping effect. In fact, as can be appreciated in **Figure 5**, a clear correlation exists between the twins' boundaries density (quantified by the perimeter density = length of twin boundaries/area (see Figure S5, Supporting Information)) and the damping of the different samples.

The figure unmistakably illustrates that the fluctuations in α values are directly linked to the boundary length of twin domains, i.e., the amount of zones with pronounced distortions of the magnetic interactions. Consequently, these regions exhibit depressed magnetic properties and act as pinning centers hindering magnetization switching. In the case of sample A, which predominantly consists of a single twin domain, the twin perimeter density is significantly smaller than that in the other samples so it appears clearly out of the observed correlation.

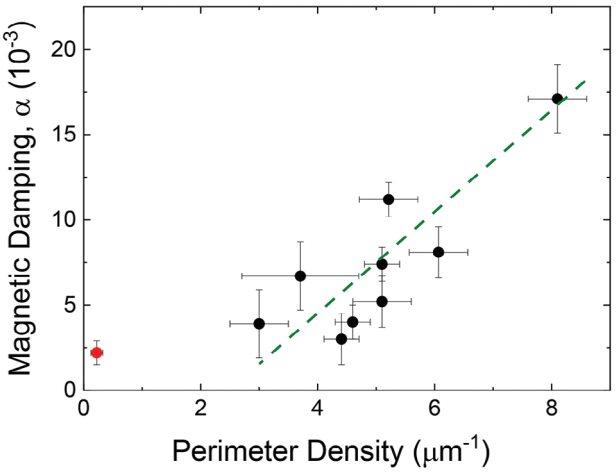

Figure 5. Dependence of the magnetic damping, α, on the amount of twin boundaries present in the different samples (twin boundaries perimeter density = perimeter of twin boundaries/area) obtained from scanning electron microscope images. The red point at the left-hand side of the graphic corresponds to sample A.

In summary, our findings underscore the complexity of optimizing damping in complex oxides, as the correlation between damping and physical properties remains unclear. Furthermore, our results reveal that conventional criteria used to assess sample quality based on DC measurements of magnetic properties (M_S and T_C) may not be the most appropriate indicators when it comes to decide on its dynamic magnetic properties.

We have demonstrated that samples with nearly identical optimal DC magnetic properties can exhibit significantly different α

values. Through a meticulous investigation, we have established a connection between damping variations and the presence of twin boundaries. These twin boundaries, where twin domains aligned along the (100) and (010) directions intersect, cause a significant degradation in magnetic properties due to the opposing rotation of MnO_6 octahedra, serving as pinning centers that impede magnetization switching. Consequently, an increase in the number of twin domains corresponds to higher magnetic damping.

Supporting Information

Supporting Information is available from the Wiley Online Library or from the author.

Acknowledgements

This work has received fundings from the "Spanish ministry of Science and Innovation" through "Severo Ochoa" (CEX2019-000917-S), "OXISOT" (PID2021-128410OB-I00) and PID2020-112914RB-I00, co-financed by the European Regional Development Fund. Shoulong Chen acknowledges financial support from the China Scholarship Council (CSC). This work has been performed in the framework of the Ph.D. program in Materials Science of the Universitat Autònoma de Barcelona (UAB), through the CSC/UAB Joint Scholarship.

Conflict of Interest

The authors declare no conflict of interest.

Author Contributions

The manuscript was written through contributions of all authors. All authors have given approval to the final version of the manuscript.

Data Availability Statement

The data that support the findings of this study are available from the corresponding author upon reasonable request.

Keywords

complex oxides, epitaxial thin films, ferromagnetic resonance spectroscopy, magnetic damping, spin dynamics

Received: October 19, 2023
Revised: November 16, 2023
Published online: December 13, 2023

[1] S. D. Bader, S. S. P. Parkin, *Annu. Rev. Condens. Matter Phys.* **2010**, *1*, 71.
[2] I. Žutic, J. Fabian, S. Das Sarma, *Rev. Mod. Phys.* **2004**, *76*, 323.
[3] H. Ebert, S. Mankovsky, D. Ködderitzsch, P. J. Kelly, *Phys. Rev. Lett.* **2011**, *107*, 66603.
[4] M. A. W. Schoen, D. Thonig, M. L. Schneider, T. J. Silva, H. T. Nembach, O. Eriksson, O. Karis, J. M. Shaw, *Nat. Phys.* **2016**, *12*, 839 .
[5] K. Gilmore, Y. U. Idzerda, M. D. Stiles, *Phys. Rev. Lett.* **2007**, *99*, 027204.
[6] B. Heinrich, C. Burrowes, E. Montoya, B. Kardasz, E. Girt, Y.-Y. Song, Y. Sun, M. Wu, *Phys. Rev. Lett.* **2011**, *107*, 066604.
[7] C. Hauser, T. Richter, N. Homonnay, C. Eisenschmidt, M. Qaid, H. Deniz, D. Hesse, M. Sawicki, S. G. Ebbinghaus, G. Schmidt, *Sci. Rep.* **2016**, *6*, 20827.
[8] S. Mizukami, D. Watanabe, M. Oogane, Y. Ando, Y. Miura, M. Shirai, T. Miyazaki, *J. Appl. Phys.* **2009**, *105*, 07D306.
[9] Y. Cui, B. Khodadadi, S. Schäfer, T. Mewes, J. Lu, S. A. Wolf, *Appl. Phys. Lett.* **2013**, *102*, 162403.
[10] L. W. Martin, Y.-H. Chu, R. Ramesh, *Mater. Sci. Eng. R* **2010**, *68*, 89.
[11] P. Zubko, S. Gariglio, M. Gabay, P. Ghosez, J.-M. Triscone, *Annu. Rev. Condens. Matter Phys.* **2011**, *2*, 141.
[12] J.-H. Park, E. Vescovo, H.-J. Kim, C. Kwon, R. Ramesh, T. Venkatesan, *Nature* **1998**, *392*, 794.
[13] C. Liu, C. K. A. Mewes, M. Chshiev, T. Mewes, W. H. Butler, *Appl. Phys. Lett.* **2009**, *95*, 022509.
[14] H. K. Lee, I. Barsukov, A. G. Swartz, B. Kim, L. Yang, H. Y. Hwang, I. N. Krivorotov, *AIP Adv.* **2016**, *6*, 055212.
[15] G. Y. Luo, C. R. Chang, J. G. Lin, *J. Appl. Phys.* **2014**, *115*, 17C508.
[16] V. Haspot, P. Noël, J. P. Attané, L. Vila, M. Bibes, A. Anane, A. Barthélémy, *Phys. Rev.* **2022**, *6*, 024406.
[17] M. Wahler, N. Homonnay, T. Richter, A. Müller, C. Eisenschmidt, B. Fuhrmann, G. Schmidt, *Sci. Rep.* **2016**, *6*, 28727.
[18] Q. Qin, S. He, W. Song, P. Yang, Q. Wu, Y. P. Feng, J. Chen, *Appl. Phys. Lett.* **2017**, *110*, 112401.
[19] T. L. Gilbert, *IEEE Trans. Magn.* **2004**, *40*, 3443.
[20] V. Kamberský, *Can. J. Phys.* **1970**, *48*, 2906.
[21] V. Kambersky, *Czech. J. Phys.* **1976**, *26*, 1366.
[22] K. Gilmore, Y. U. Idzerda, M. D. Stiles, *J. Appl. Phys.* **2008**, *103*, 07D303.
[23] F. Sandiumenge, J. Santiso, L. Balcells, Z. Konstantinovic, J. Roqueta, A. Pomar, J. P. Espinós, B. Martínez, *Phys. Rev. Lett.* **2013**, *110*, 107206.
[24] J. M. Vila-Fungueiriño, C. T. Bui, B. Rivas-Murias, E. Winkler, J. Milano, J. Santiso, F. Rivadulla, *J. Phys. D: Appl. Phys.* **2016**, *49*, 315001.
[25] U. Gebhardt, N. V. Kasper, A. Vigliante, P. Wochner, H. Dosch, F. S. Razavi, H.-U. Habermeier, *Phys. Rev. Lett.* **2007**, *98*, 096101.
[26] P. Stamenov, J. M. D. Coey, *Rev. Sci. Instrum.* **2006**, *77*, 015106.
[27] M. Farle, *Rep. Prog. Phys.* **1998**, *61*, 755.
[28] Y. Suzuki, H. Y. Hwang, S.-W. Cheong, T. Siegrist, R. B. Van Dover, A. Asamitsu, Y. Tokura, *J. Appl. Phys.* **1998**, *83*, 7064.
[29] S. E. Lofland, S. M. Bhagat, C. Kwon, S. D. Tyagi, Y. M. Mukovskii, S. G. Karabashev, A. M. Balbashov, *J. Appl. Phys.* **1997**, *81*, 5737.
[30] A. Vailionis, H. Boschker, W. Siemons, E. P. Houwman, D. H. A. Blank, G. Rijnders, G. Koster, *Phys. Rev. B* **2011**, *83*, 064101.
[31] K. Steenbeck, R. Hiergeist, *Appl. Phys. Lett.* **1999**, *75*, 1778.
[32] L. Balcells, M. Paradinas, N. Baguès, N. Domingo, R. Moreno, R. Galceran, M. Walls, J. Santiso, Z. Konstantinovic, A. Pomar, M.-J. Casanove, C. Ocal, B. Martínez, F. Sandiumenge, *Phys. Rev. B* **2015**, *92*, 075111.
[33] J. Santiso, L. Balcells, Z. Konstantinovic, J. Roqueta, P. Ferrer, A. Pomar, B. Martínez, F. Sandiumenge, *CrystEngComm* **2013**, *15*, 3908.
[34] L. I. Koroleva, R. V. Demin, A. M. Balbashov, *JETP Lett.* **1997**, *65*, 474.